Electrocatalysis (2016) 7:22–32
DOI 10.1007/s12678-015-0277-7

ORIGINAL RESEARCH

PtAu Electrocatalyst for Glycerol Oxidation Reaction Using a ATR-FTIR/Single Direct Alkaline Glycerol/Air Cell In Situ Study

Cristiane Angélica Ottoni[1] · **Sirlane G. da Silva**[1] · **Rodrigo F. B. De Souza**[1] · **Almir Oliveira Neto**[1]

Published online: 3 September 2015

Abstract Different ratios of PtAu/C electrocatalysts were synthesized and assessed for their capability by glycerol electrooxidation. Electrocatalysts were characterized by X-ray diffraction (XRD), transmission electron microscopy (TEM), cyclic voltammetry (CV), chronoamperometry, and direct glycerol/air fuel cell coupled with a ATR-FTIR setup. XRD of PtAu/C electrocatalysts showed the presence of Pt (fcc), Au (fcc), and PtAu (fcc) phases, and TEM images for PtAu/C electrocatalysts showed particle size between 5.4 and 5.8 nm. PtAu/C (50:50) presented the best result for glycerol electrooxidation by cyclic voltammetry and chronoamperommetry measurements in comparison with other electrocatalysts prepared. All PtAu/C showed better performance in comparison with Pt/C and Au/C. Moreover, the addition of gold to platinum favored glycerol by electronic effect and bifunctional mechanism. Through ATR-FTIR/direct alkaline glycerol/air cell in-situ study, it was possible to identify glycerate and tartronate as main products formed during the electrochemical glycerol oxidation.

Keywords PtAu/C electrocatalysts · Alkaline fuel cell · Glycerol

✉ Almir Oliveira Neto
aolivei@ipen.br

[1] Instituto de Pesquisas Energéticas e Nucleares, IPEN/CNEN-SP, Av. Prof. Lineu Prestes, 2242 Cidade Universitária, CEP 05508-900 São Paulo, SP, Brazil

Introduction

In the last decades, several types of fuel cells have been developed and investigated as a promising technology capable of converting chemical energy into electrical energy. Direct liquid fuel cell (DLFC) has great potential for mobile use mainly due to the fact that it can be constructed in compact form and dispense other accessorial devices such as a reformer or a tank for pure gases. From among the existent DLFC, we highlight the alcohol/air cells that have been studied for portable applications, operating at room temperature and atmospheric air and exempt of moving parts [1].

Methanol has been extensively studied in direct methanol fuel cell in the last three decades, even though it is toxic, volatile, and flammable [2–4]. Recently, other alcohols are being used in this approach, some of those being ethanol [5–7], ethylene glycol [8], and glycerol [7].

Glycerol, one of the referred fuels and a byproduct of biodiesel, is a very attractive choice due to its low toxicity and high energy density. It can provide up to 14 electrons per molecule, come from a renewable source (biomass), be less susceptible to crossover and be relatively inexpensive [9–11]. During the electrooxidation process, a great number of intermediates can be generated which can poison the catalytic site thus decreasing the activity of the electrocatalyst.

For the electrooxidation of glycerol, Pt [10, 12, 13], Pd [12–14], and Au [13, 15–17] are the most investigated metals, beyond the binary or ternary materials [9, 11, 12], containing or not these noble metals. It is known that, in both acidic and alkaline conditions, some oxygen species have affinity for adsorbing Pt at sites, which is an essential metal in fuel cells that has high chemical and electrochemical stability [18–21]. Au, which also has chemical and electrochemical stability,

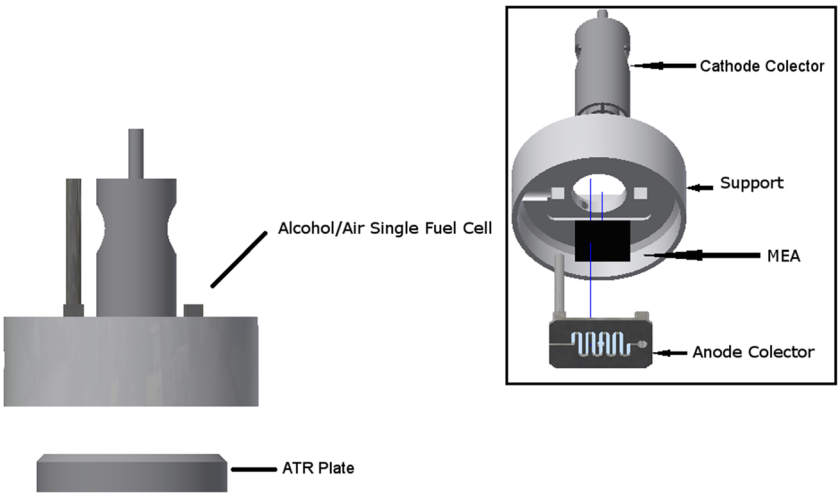

Fig. 1 ATR-FTIR/alcohol/air single cell setup

has affinity for OH groups that make the Au surface hydroxylated in alkaline medium and interaction of alkoxide an obligatory way [17].

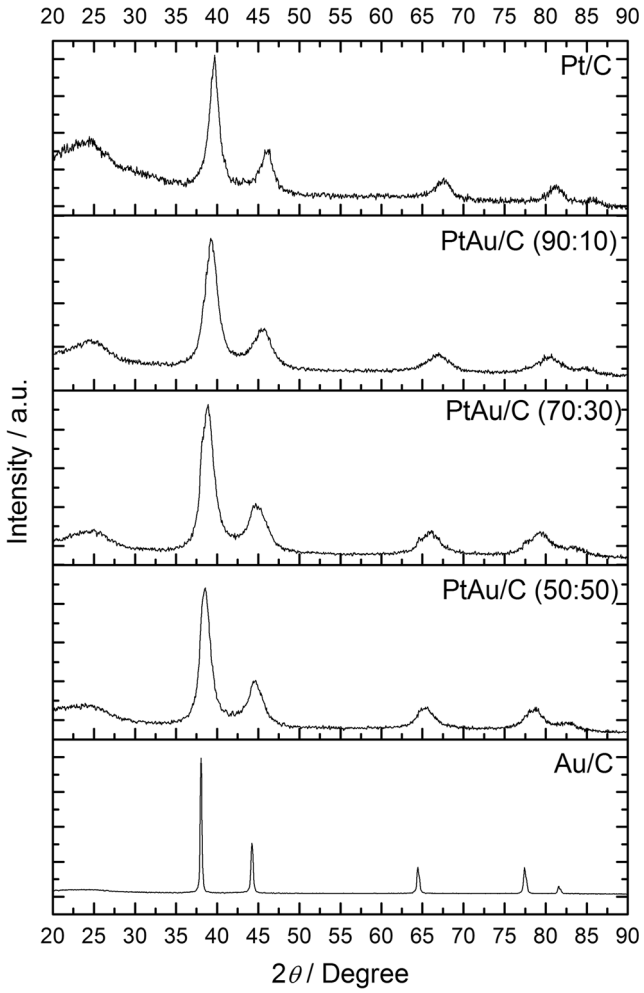

Fig. 2 X-ray diffractograms of Pt/C, PtAu/C (90:10), PtAu/C (70:30), PtAu/C (50:50), and Au/C electrocatalysts

Several studies evaluated glycerol oxidation performance under alkaline and acidic conditions, showing that a better performance occurs under alkaline conditions in comparison with acidic conditions [10, 12, 17, 22, 23]. This fact is associated with primary hydroxyl favoring in detriment of secondary hydroxyl and consequent promotion of a kinetics reaction increment, beyond the deprotonation of these groups due to the high pH [10, 12, 17]. However, the principal products of reaction have not been identified during the operation of a glycerol fuel cell using ATR-FTIR/single direct alkaline glycerol/air cell.

In this context, PtAu/C electrocatalysts with different Pt/Au atomic ratios were tested for glycerol electrooxidation in alkaline medium, using electrochemical techniques at room temperature. The products and intermediates formed as a result of the glycerol electrooxidation were determined for the first time using ATR-FTIR/single direct alkaline glycerol/air cell.

Experimental Procedures

As previously described by Neto et al [24–26], the borohydride reduction method was used to prepare electrocatalysts: PtAu/C (20 wt% of metals loading in different atomic ratio PtAu/C (50:50), PtAu/C (70:30), and PtAu/C (90:10)), $H_2PtCl_6.6H_2O$ (Aldrich), and $HAuCl_4.3H_2O$ (Aldrich) were the metal sources and Carbon Vulcan XC72 was the support structure. Initially, Carbon Vulcan XC72 was dispersed in a solution of isopropyl alcohol/water (50/50, *v*/*v*) followed by metal sources addition and posterior maintenance in ultrasonic bath for 10 min. Then, $NaBH_4$ was diluted in 0.01 mol L^{-1} NaOH solution. Finally, the resulting solution was stirred for 30 min at room temperature. The mixture was filtered, and the resulting solids were washed with distilled water and dried at 70 °C for 2 h. Analytical

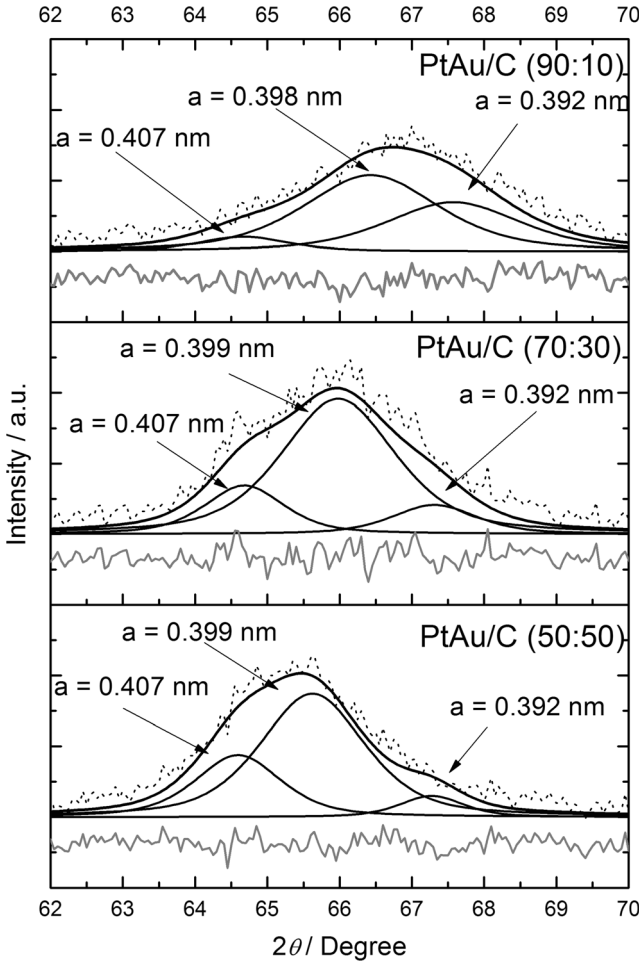

Fig. 3 Pawley refinement of peak (2 2 0) in all diffratograms with *dot* for experimental measure, *line* for modeled, and *gray line* for residual

technique X-ray diffraction (XRD) (Rigaku diffractometer model Miniflex II, using Cu Ka radiation source −0.15406 nm) was applied to characterize the synthesized material.

The X-ray diffraction patterns were recorded in the range of 2 20°–90° with a step size of 0.05° and a scan time of 2 s per step. The electrocatalyst structures were analyzed by scanning electron microscopy (TEM, transmission electron microscopy JEM-2100) operated at 200 kV. Distribution particles histogram was determined by 100 particles measurements from a micrograph.

Electrochemical assays were carried out using a three-electrode conventional cell, where the reference electrode and counter electrode utilized were Ag/AgCl (3 mol L^{-1} KCl) and Pt wire, respectively. Thin porous coating technique (cavity 0.30 mm deep and 0.36 cm^2 area) was used as working electrode. The electrode was prepared with 20 mg of the electrocatalyst, and it was added in 50 mL of water containing three drops of a 6 % polytetrafluoroethylene (PTFE) suspension. After that, the mixture was treated in an ultrasound bath for 10 min, filtered, and attached in the working electrode. For electrochemical characterizations, cyclic voltammetry and chronoamperommetry technics were utilized. The cyclic voltammetry analyses were conducted at a scan rate of $10mVs^{-1}$ in KOH (1 mol L^{-1}) in the presence and absence of glycerol (1 mol L^{-1}), while that of chronoamperometry (amperometric curves) were recorded in the same electrolyte containing glycerol at −0.35 V for 1800 s. All measurements were conducted at room temperature.

Single direct alkaline glycerol/air cell tests were carried out using PtAu materials based as an anode, and Pt/C BASF (20 wt%) electrocatalysts as the cathode in the gas diffusion electrodes. The electrocatalyst was painted over the gas diffusion layer (Carbon Paper Teflon treated Electrochem EC-TP1-060T) in order to obtain a homogeneous dispersion made with Nafion solution (5 wt%, Aldrich) and isopropanol (J.T. Baker). All electrodes were constructed with 1 mg metal cm^{-2}. After preparation, the electrodes were hot pressed on both sides of a Nafion 117 membrane at 125 °C for 2 min under a pressure of 225 kgf cm^{-2}.

The performance and ATR-FTIR in situ spectroscopy of the single direct alkaline glycerol/air cell was investigated using a special single cell (Fig. 1) based in a single fuel cell/ATR-FTIR previously showed in the literature [27, 28]. This had a geometric area of 1 cm^2, was adapted in an ATR accessory (MIRacle with a Diamond/ZnSe Crystal Plate Pike), and was installed on a Nicolet 6700 FTIR spectrometer equipped with a MCT detector cooled with liquid N_2.

The detection of the spectra for each potential was carried out using a solution of 1 mol L^{-1} glycerol+ 1 mol L^{-1} KOH. The fuel was replaced after the collection of each spectrum. The assays were performed at a temperature of 25 °C. The polarization curves were obtained using an Autolab PGSTAT 302 N Potentiostat. The spectra were computed from 128 interferograms averaged from 4000 to 900 cm^{-1} with the spectral resolution set to 4 cm^{-1}. Absorbance spectra were collected as the ratio R/R_0, where R represents a spectrum at a given potential and R_0 is the spectrum collected at an open-circuit voltage (OCV). Negative and positive bands represent the consumption and production of substances, respectively.

Results and Discussion

PtAu electrocatalysts, prepared in the atomic ratio 100:0, 90:10, 70:30, 50:50, and 0:100 were analyzed by X-ray diffractograms (Fig. 2). For all materials analyzed, peaks at 2θ degree near to 39, 46, 67, and 81 were detected, and these are associated with the planes (111), (200), (220), and (311)

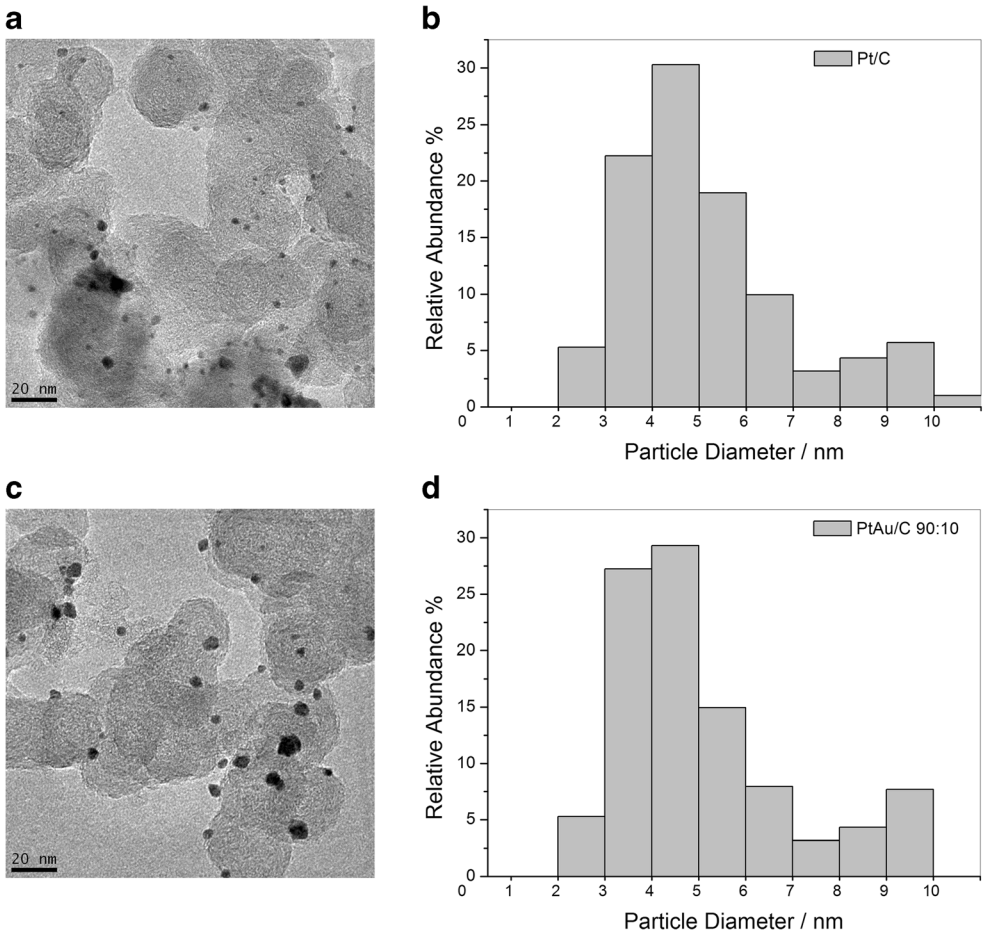

Fig. 4 TEM micrographs and histograms of the particle size distribution of Pt/C, PtAu/C (90:10), PtAu/C (70:30), PtAu/C (50:50), and Au/C

characteristic of the face-centered cubic structure platinum (JCPDF 89-7382) [29] and gold (JCPDF 89-3697) [25]. It is also possible to observe a broad peak at about 25 associated with the hexagonal structure Vulcan XC72 carbon [30, 31].

The platinum-containing materials present a diffraction peak expanded when compared to the Au/C. This characteristic can indicate a larger average crystallite size, which was estimated by the Debye-Scherrer equation [32, 33]. According to the results of 4 nm (Pt/C), 4 nm (PtAu/C 90:10), 5 nm (PtAu/C ⁻70:30), 6 nm (PtAu/C −50:50), and 14 nm (Au/C), there is a direct relationship, previously described in literature [31, 32], between the amount of gold used in the composition of the electrocatalyst and the size of the formed nanoparticles.

Another important aspect observed in the region of the diffraction plane peak (220), by materials containing Pt and Au, was a shift to less positive values with the increment in the amount of gold in the electrocatalyst. To obtain more information regarding these peaks with respect to the lattice parameters, the XRD patterns were refined using the Pawley method [34] carried out with Fityk 0.98 software, as reported by Wojdyr [35] (Fig. 3). The displacement peak was a result of the decreasing participation of Pt phase (a=0392 nm), the increasing contribution of the peaks relating phases of Au (a= 0407 nm) indicating a PtAu alloy (a≈0398 nm), and the increment of PtAu alloy in the catalyst that cause the peak shift.

TEM images and the histogram of the Pt/C, PtAu/C, and Au/C materials are shown in Fig. 4. PtAu/C materials had a good distribution on the carbon support; however, there were some agglomerations. Au/C materials showed a heterogeneous distribution with larger and more agglomerated particles. The particles' size average calculated from the histograms were 16 nm (Au/C), 5.8 nm (PtAu/C (50:50)), 5.2 nm (PtAu/C (70:30)), 5.4 nm (PtAu/C (90:10)), and 5.1 nm (Pt/C), confirming the data obtained by X-ray diffraction.

In Fig. 5, cyclic voltammograms (CV) of Pt/C, PtAu/C, and Au/C electrocatalysts are presented. The hydrogen adsorption/desorption peaks of Pt are well defined in the interval of ⁻0.85 to ⁻0.5 V [26]. The intensity of these peaks decreased in PtAu electrocatalysts with the increase of Au content; therefore, this behavior indicates that there is coverage of platinum active sites by gold, as an occurrence with other transition metals

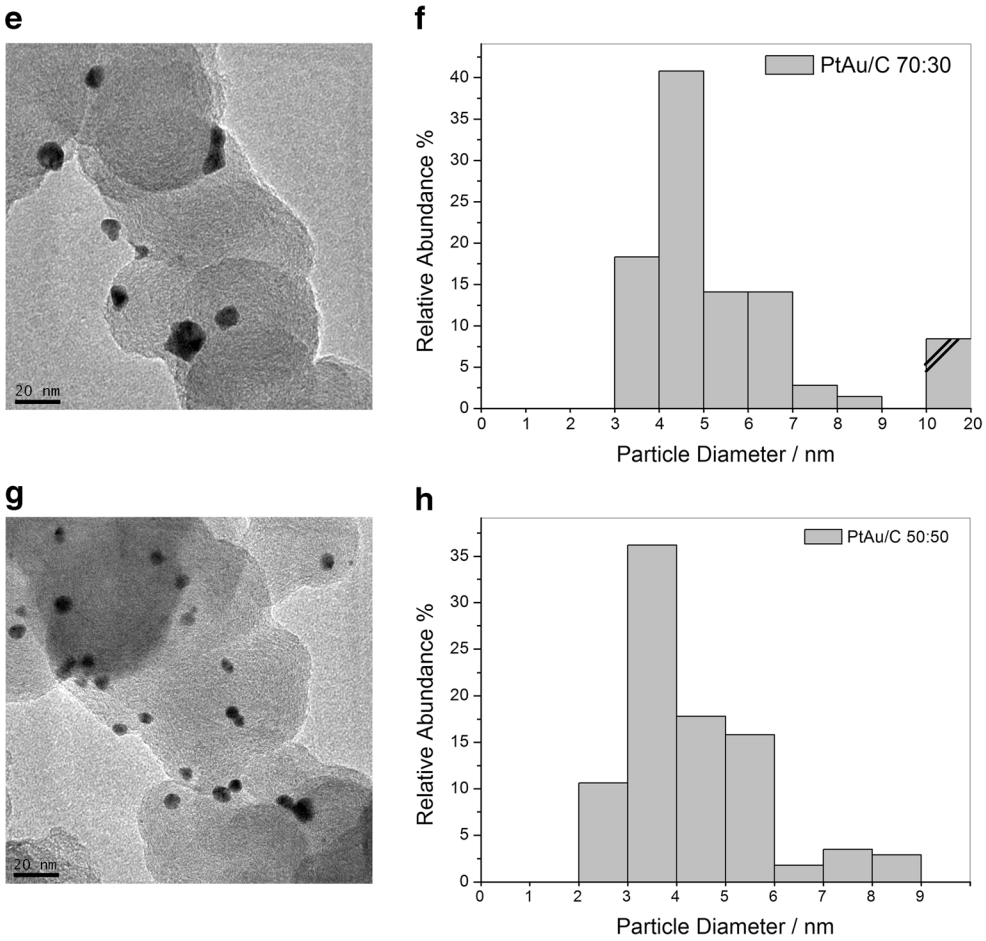

Fig. 4 continued.

[36]. Gold does not absorb hydrogen in this potential region, as can be observed for the Au/C material.

Figure 6a shows the CV of Pt/C, Au/C, and PtAu/C with different atomic ratios 90:10, 70:30, and 50:50 in the presence of glycerol (1.0 mol L^{-1}) and KOH (1.0 mol L^{-1}) solutions, where the CVs were normalized by the amount of metal in the electrocatalysts.

The CV of PtAu/C 70:30 and PtAu/C 50:50 electrocatalyst presented lower onset potential (−0.68 V vs. Ag/AgCl) when compared to PtAu/C 90:10 and Pt/C (−0.60 V vs. Ag/AgCl). Meanwhile, Au/C electrocatalyst showed a higher onset potential (−0.55 V vs. Ag/AgCl). PtAu/C (50:50) showed best performance towards glycerol electrooxidation in comparison with all electrocatalysts prepared, while Au/C showed the lowest performance. All PtAu/C electrocatalysts prepared were more active for glycerol oxidation than Pt/C. These results indicate that addition of Au to Pt favors the reaction by electronic effect (electronic modification of Pt) and bifunctional mechanism (activation of interfacial water molecules at lower potentials than in the case of pure Pt).

Chronoamperometry curves (Fig. 6b) were recorded in the presence of the KOH (1.0 mol L^{-1}) in glycerol (1.0 mol L^{-1}) solution at a fixed potential of −0.35 V vs. Ag/AgCl for Pt/C, Au/C, and PtAu/C during 30 min. By chronoamperommetry, the binary materials prepared were also more active than only Pt/C and Au/C. The final currents values at −0.35 V were: PtAu/C 50:50 (10:15 mA mg^{-1})>PtAu/C 70:30 (8.3 mA mg^{-1})>PtAu/C 90:10 (7.9 mA mg^{-1})>Pt/C (5.6 mA mg^{-1})>Au/C (2.4 mg mA^{-1}).

Electrochemical experiments for materials based on Pt and Au indicate that binary materials are more active for glycerol oxidation due to a synergistic effect of alcohol adsorption with Pt [15], where the Au acts in the indirect oxidation decreasing the amount of adsorbed species on Pt providing OH species to oxidize them faster [37]. Therefore, high pH values promote alkoxides interactions that are attracted by the species present in hydroxilated surface gold. However, both possibilities can exist without invalidating each other [15].

The performance of a single alcohol/air cell adapted in an ATR setup for the different electrocatalysts is presented in Fig. 7. The OCV (Fig. 7a.) of the Pt-, PtAu-, and Au-based materials is 0.55 V for PtAu/C 90:10, 0.52 V for Au/C and PtAu/C 50:50, 0.42 V for Pt/C, and 0.39 V for PtAu/C 70:30.

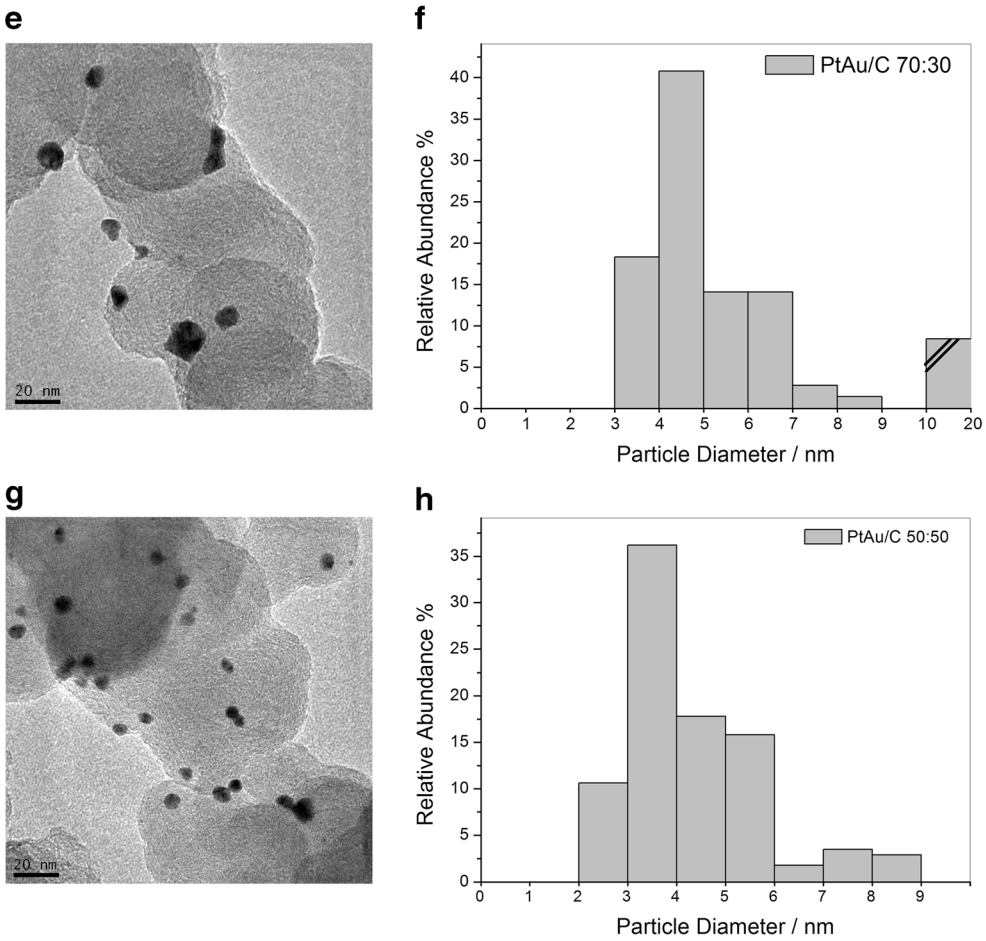

Fig. 4 continued.

The power curves (Fig. 7b) obtained in the accompanying electrochemical experiments indicate that PtAu/C 50:50 is more active than the other materials (0.51 mW cm^{-2}), followed by PtAu/C 90:10 (0.45 mW cm^{-2}), PtAu/C 70:30 (0.41 mW cm^{-2}), Pt/C (0:40 mW cm^{-2}), and Au/C (0:38 mW cm^{-2}).

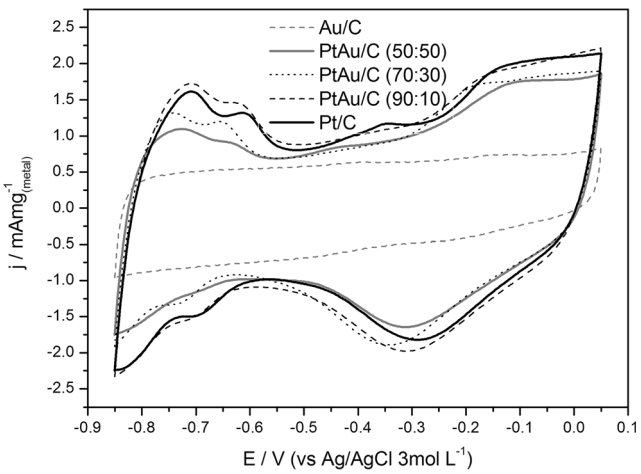

Fig. 5 Cyclic voltammetry of Pt/C, Au/C, and PtAu/C electrocatalysts in 1 mol L^{-1} KOH solution with a scan rate of 10 mV s^{-1} at 25 °C

The ATR-FTIR spectra (Fig. 8) were acquired during the experiments of polarization curves (Fig. 7) on the anode side of the single fuel, operating with glycerol+KOH aqueous solution, to correlate the activity of glycerol electrooxidation with the preferential mechanism.

ATR-FTIR analyses were performed for Pt/C, PtAu/C, and Au/C to identify the products of glycerol electrooxidation during the potential scan between OCV and 0.0 V. The IR spectra were recorded every 0.05 V, in glycerol (1.0 mol L^{-1}) and KOH (1.0 mol L^{-1}) aqueous solution.

For these spectra, a decrease of the glycerol bands (1004, 1041, and 1094 cm^{-1}) [9, 38] with an increase of the potential indicating glycerol consumption was observed. An increase of the bands resulting from 1377 cm^{-1} corresponding to glycerate [23, 39, 40], 1340 cm^{-1} to tartronate [41], 1335 cm^{-1} to 1,3-Dihydroxy-2-propanone [40], 1353 cm^{-1} to hydroxypyruvate [9, 38], 1225 cm^{-1} to formate, ~1405 cm^{-1} to carbonate [9], ~1589 cm^{-1} to H-O-H

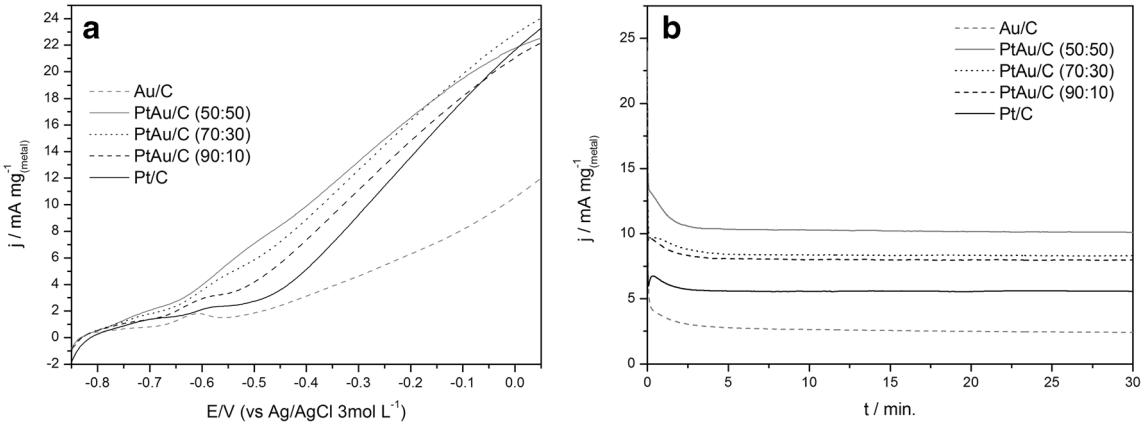

Fig. 6 **a** Cyclic voltammetry of Pt/C, Au/C, and PtAu/C electrocatalysts at atomic ratios 90:10, 70:30, and 50:50 in 1.0 mol L^{-1} KOH in 1.0 mol L^{-1} glycerol, in a potential range from −0.85 to 0.10 V vs. Ag/AgCl, at a scan rate of 10 mV s^{-1}. **b** Current-time curves at −0.30 V for Pt/C, Au/C, and PtAu/C electrocatalysts, at atomic ratios 90:10, 70:30, and 50:50 in 1.0 mol L^{-1} glycerol in 1.0 mol L^{-1} KOH

deformation, symmetric COO^- stretch to glycolate and glyoxylate [9], ~1665 cm^{-1} to carbonyl and carboxyl stretches [9, 39], and 1723 cm^{-1} to carboxyl stretching [9, 42] was also observed. CO_2 signal (2343 cm^{-1}) [27] was not detected in these spectra, and glyceraldehyde bands (1071 cm^{-1}) were not found; these were probably due to low stability of the primary aldehydes under alkaline condition [17].

During the fuel cell experiments, as the current increased, there was an increase in the glycerol consumption (negative bands) and consequently there was the formation of other species. In order to evaluate the catalyst composition effect in the products with the application of different potentials, all bands were deconvoluted to Lorentzian line forms [43]. Figure 9 shows the integrated intensities of the bands for glycerate (1377 cm^{-1}) and tartronate (1345 cm^{-1}), being possible to observe that the formation of glycerate presents a profile that increases towards the OCV to 0 V. The tartronate formation, for the majority of Pt Au materials, showed a less positive potential in comparison with other products. It was observed the onset with a great increase in the first potential and then production was attenuated, but this still increased with the final potential. In the literature, it is described that the tartronate is a product of the oxidation of glycerate [23, 40]. However, the production profile of both compounds (glycerate and tartorate) can indicate that they can be produced in a parallel mechanism, since we observed a tendency to decrease in the glycerate formation with the beginning of production of the tartronate.

For the electrocatalyst PtAu/C 90:10, no bands were observed for the hydroxypyruvate and 1,3-dihydroxy-2-propanone, indicating that this material promotes the production pathway of carboxilates, glycerate and tartronate produced simultaneously just to OCV. Figure 10 shows band integrations of hydroxypyruvate and 1,3-dihydroxy-2-propanone as a potential function. In electrochemical cell experiments, performed in three different electrodes suitable for electrochemical cells, the

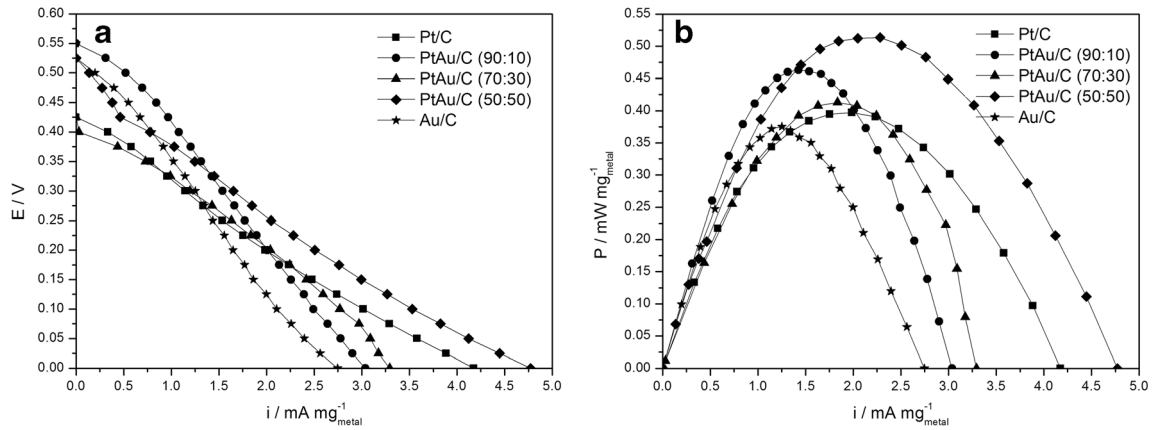

Fig. 7 Polarization curves of single direct alkaline glycerol/air cell for Pt/C, Au/C, and PtAu/C electrocatalysts at atomic ratios 90:10, 70:30, and 50:50

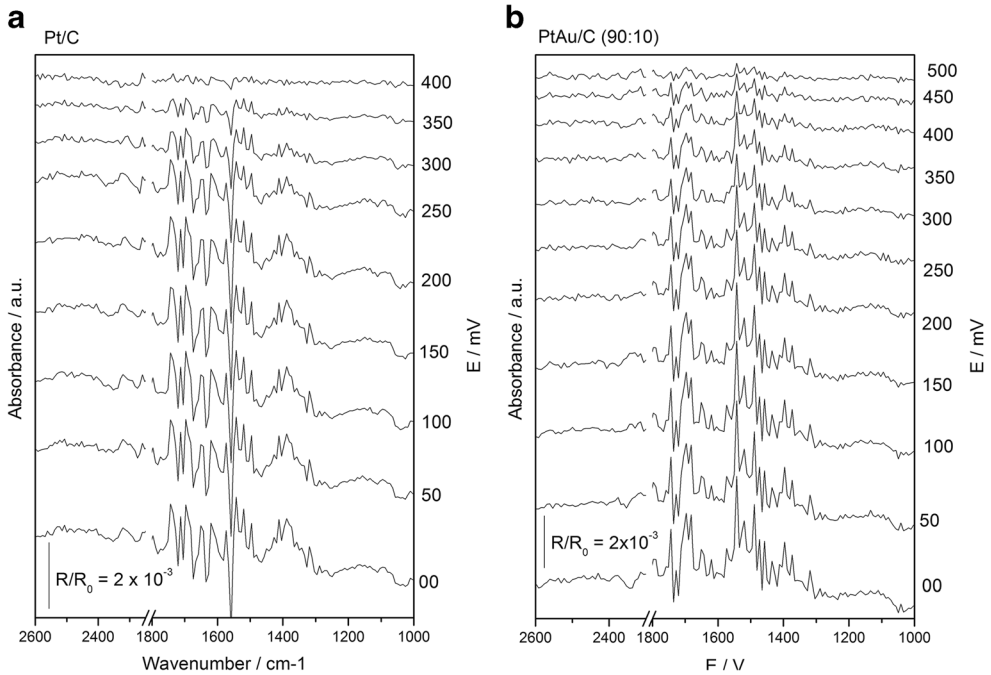

Fig. 8 ATR-FTIR/single direct alkaline glycerol/air cell for Pt/C, PtAu/C, and Au/C electrocatalysts in 1.0 mol L^{-1} glycerol in 1.0 mol L^{-1} KOH. Each spectrum corresponds to an increase of 0.05 V

point hydroxypyruvate is a product of oxidation of the 1,3-dihydroxy-2-propanone [40]. However, we saw that in these experiments, using a single glycerol/air fuel cell, these products are produced in parallel. Except for Au/C, it is possible to note that the reduction in potential from these products is close to 0 V. The

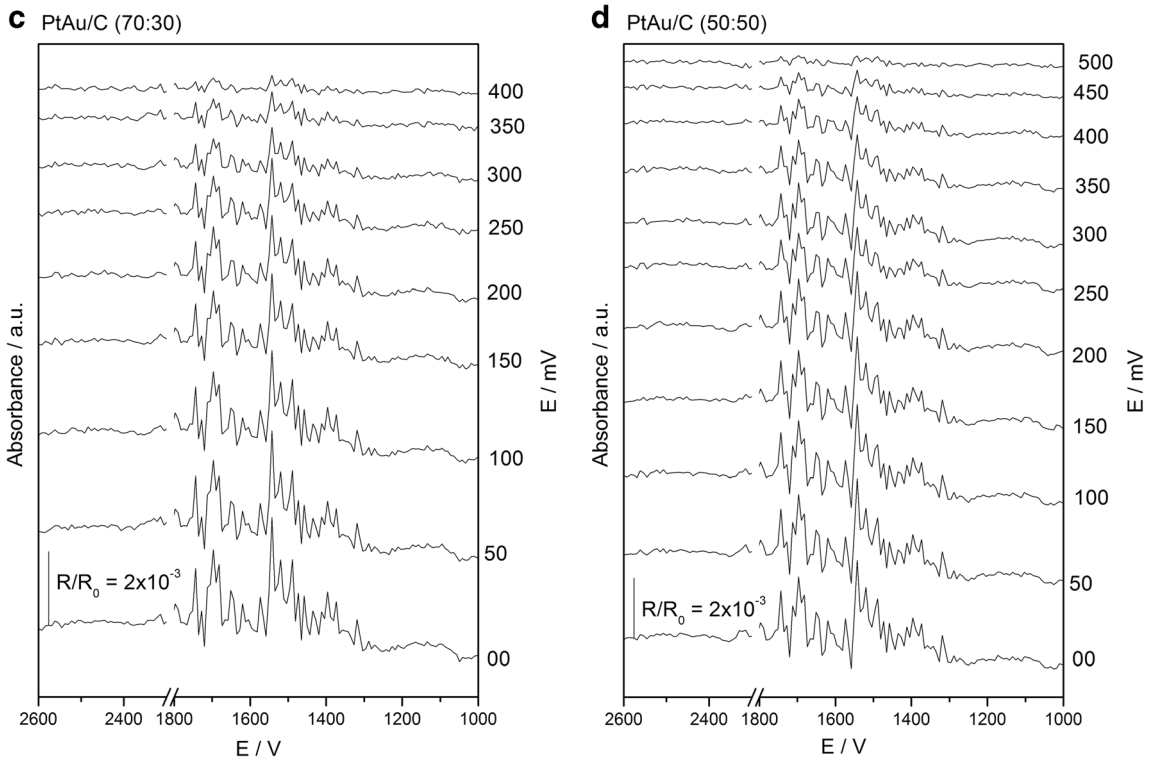

Fig. 8 continued.

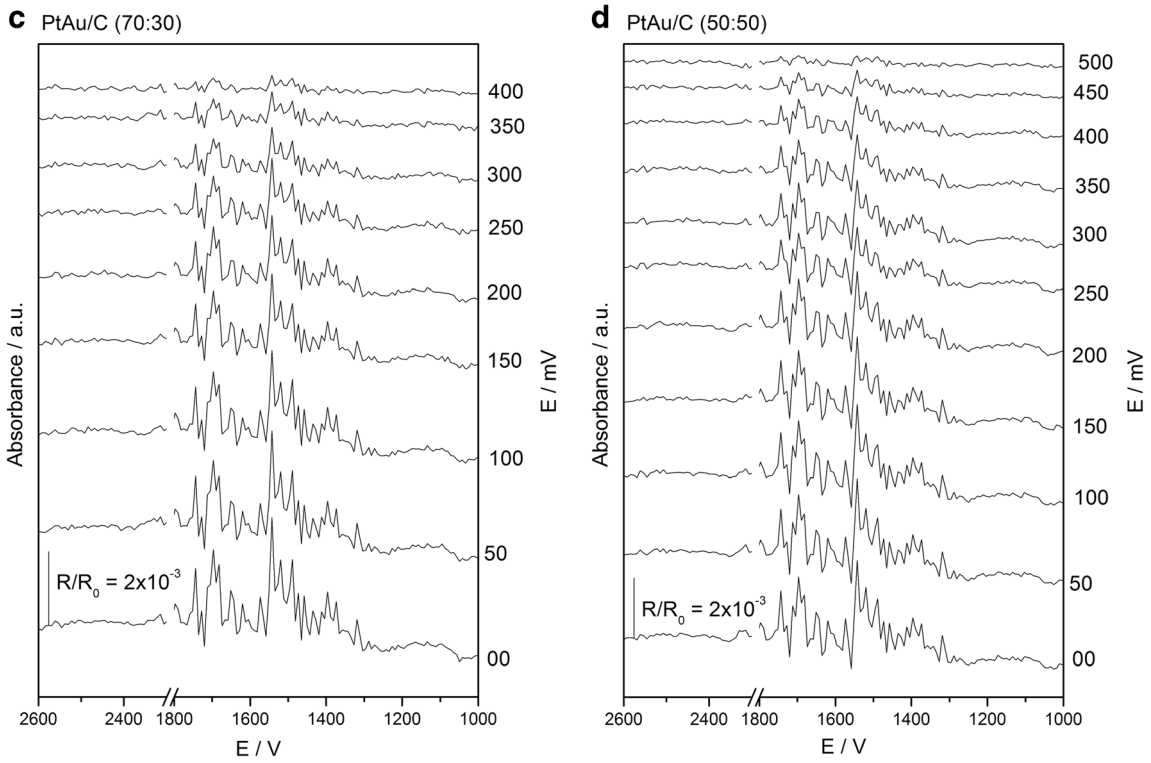

Fig. 8 continued.

continuous production of less oxidized products may be one explanation for the reduced power density measured for this material.

When analyzing glycolate production (Fig. 11), it is possible to observe that the potential onset is closer to the OCV for all catalysts, highlighting the PtAu/C 50:50 material that has the highest intensity production of this specie in potential near the maximum power density. It is commonly reported that the glycolate oxidation produces oxalate [16, 44]. For the materials studied, this specie appears with an approximate potential of 100 mV less positive than the OCV. Except for PtAu/C (90:10), where glycolate and oxalate bands start to decrease after a certain potential, becoming extinguished in the case of Pt 0 V.

For compound C_1, we detected bands relating to formate and carbonate. In the potential near its OCV, the formate was detected for all materials containing Au. Materials that had more than 30 % gold in their composition had an initial increment production of this specie and they then presented a potential consumption until they reached a constant concentration. This result indicates that Au favors the cleavage of C-C. And, although CO_2 was not detected for Au/C, carbonate bands

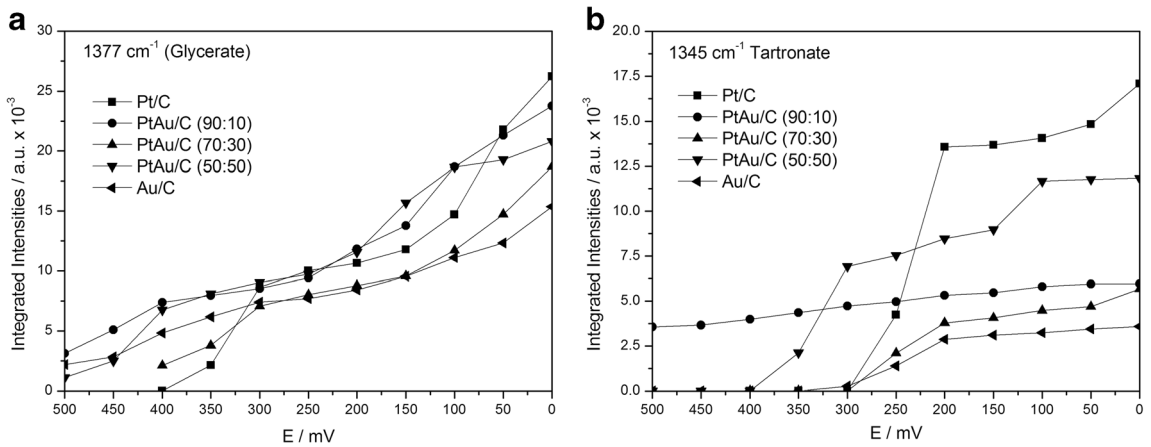

Fig. 9 Glycerate and tartronate integrated intensities bands as a function of the potential. Data extracted from Fig. 8

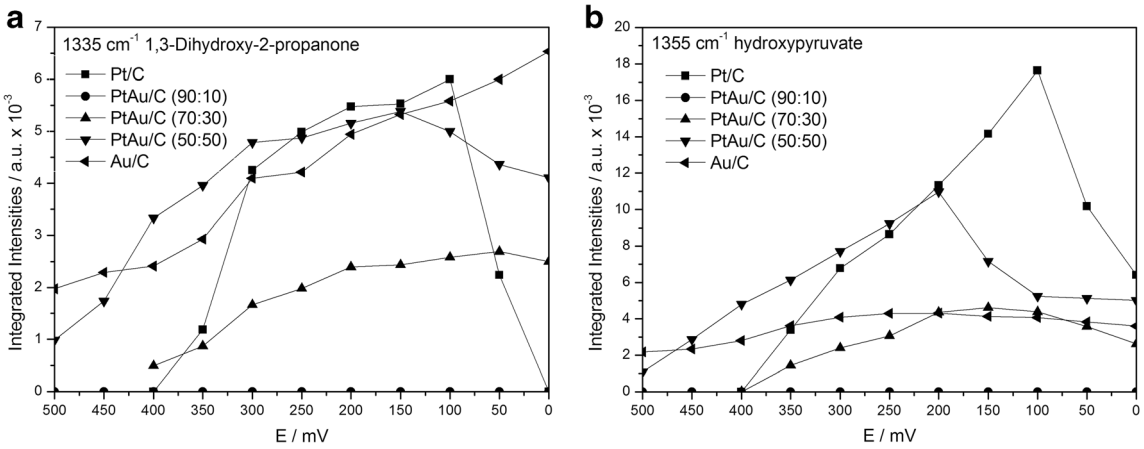

Fig. 10 1,3-dihydroxy-2-propanone and hydroxypyruvate integrated intensities bands as a function of the potential. Data extracted from Fig. 8

production with highest intensity relating to CO_2 precipitated was detected, due to the alkaline medium.

Although Zhang et al [10] detected the presence of mexolate, by liquid chromatography, when working with Pt/C in a unit cell, in our experiments we did not find any bands characteristic of this product.

The results obtained for the ATR-FTIR in a single glycerol/air fuel cell indicate that the potential for the spontaneous activation of the cell is sufficient for the production of several species in different oxidation states contrary to those reported in literature for three different electrodes of electrochemical cells [23].

Conclusion

Our choice of the borohydride reduction process to produce PtAu/C for glycerol oxidation proved to be an effective method. DRX of PtAu/C electrocatalysts showed the presence of Pt (fcc), Au (fcc), and PtAu (fcc) alloy phases. It also showed an increase in Au content on the PtAu/C electrocatalysts which resulted in an increase on the PtAu alloy phase. TEM micrographs showed a good distribution of the nanoparticles on the carbon support with average particle sizes in the range of 5–6 nm.

All PtAu/C electrocatalysts exhibited higher performances for glycerol oxidation in alkaline media when compared to Pt/C and Au/C at room temperature. This effect may be associated with the electronic effect and bifunctional mechanism observed by DRX and cyclic voltammetry analyses. The promoting effect of the second metal on PtAu/C could also be explained by a higher formation of glycerate and tartronate observed by ATR-FTIR in a single glycerol/air fuel cell.

We also observed that the presence of Au favors the breaking of the C-C bond, producing more carbonate than other materials. However, the complete oxidation kinetics is slower, which reflects a lesser current density. The excellent results obtained by PtAu/C electrocatalysts provide a good basis for further evaluation studies.

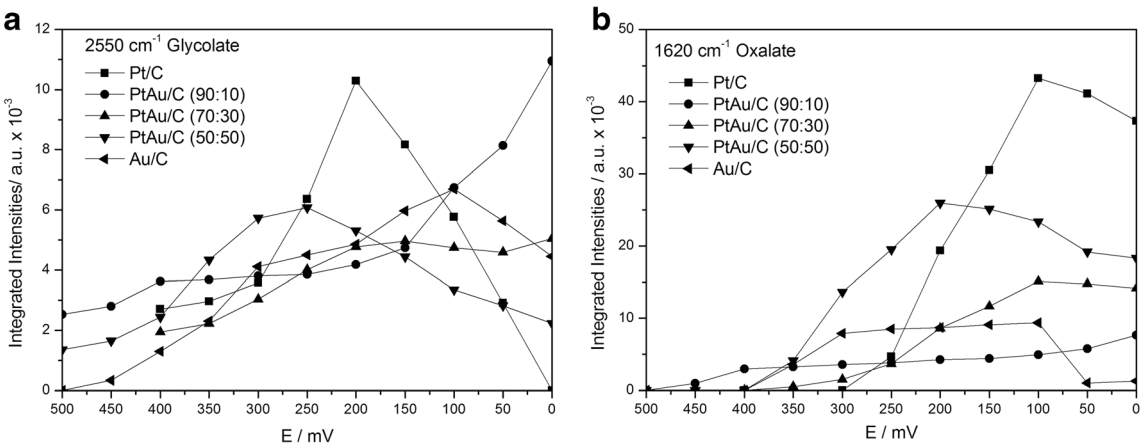

Fig. 11 Glycolate, oxalate, formate, and carbonate integrated intensities bands as a function of the potential. Data extracted from Fig. 8

Acknowledgments The authors thank CNPq (150111/2015-0) and CAPES for financial support and CCTM from IPEN/CNEN-SP for TEM measurements.

Reference

1. B.D. McNicol, D.A.J. Rand, K.R. Williams, J. Power Sources **83**, 15–31 (1999)
2. L. An, T.S. Zhao, S.Y. Shen, Q.X. Wu, R. Chen, Int. J. Hydrog. Energy. **35**, 4329–4335 (2010)
3. J.M. Sieben, M.M.E. Duarte, Int. J. Hydrog. Energy. **36**, 3313–3321 (2011)
4. T. Yuan, J. Yang, Y. Wang, H. Ding, X. Li, L. Liu, H. Yang, Electrochim. Acta **147**, 265–270 (2014)
5. V. Bambagioni, C. Bianchini, Y. Chen, J. Filippi, P. Fornasiero, M. Innocenti, A. Lavacchi, A. Marchionni, W. Oberhauser, F. Vizza, ChemSusChem **5**, 1266–1273 (2012)
6. J.P. Pereira, D.S. Falcão, V.B. Oliveira, A.M.F.R. Pinto, J. Power Sources **256**, 14–19 (2014)
7. V. Bambagioni, C. Bianchini, A. Marchionni, J. Filippi, F. Vizza, J. Teddy, P. Serp, M. Zhiani, J. Power Sources **190**, 241–251 (2009)
8. J.R. Varcoe, R.C.T. Slade, E.L.H. Yee, S.D. Poynton, D.J. Driscoll, J. Power Sources **173**, 194–199 (2007)
9. A. Falase, M. Main, K. Garcia, A. Serov, C. Lau, P. Atanassov, Electrochim. Acta **66**, 295–301 (2012)
10. Z. Zhang, L. Xin, W. Li, Appl. Catal. B. **119–120**, 40–48 (2012)
11. C. Chen, S. Zhu, X. Yang, L. Pi, Z. Cui, Electrochim. Acta **56**, 10253–10258 (2011)
12. A. Ilie, M. Simoes, S. Baranton, C. Coutanceau, S. Martemianov, J. Power Sources **196**, 4965–4971 (2011)
13. Z. Zhang, L. Xin, J. Qi, D.J. Chadderdon, W. Li, Appl. Catal. B. **136–137**, 29–39 (2013)
14. A. Dector, F.M. Cuevas-Muñiz, M. Guerra-Balcázar, L.A. Godínez, J. Ledesma-García, L.G. Arriaga, Int. J. Hydrog. Energy. **38**, 12617–12622 (2013)
15. J. Qi, L. Xin, D.J. Chadderdon, Y. Qiu, Y. Jiang, N. Benipal, C. Liang, W. Li, Appl. Catal. B. **154–155**, 360–368 (2014)
16. L. Xin, Z. Zhang, J. Qi, D. Chadderdon, W. Li, Appl. Catal. B. **125**, 85–94 (2012)
17. Y. Kwon, S.C.S. Lai, P. Rodriguez, M.T.M. Koper, J. Am. Chem. Soc. **133**, 6914–6917 (2011)
18. W.J. Zhou, B. Zhou, W.Z. Li, Z.H. Zhou, S.Q. Song, G.Q. Sun, Q. Xin, S. Douvartzides, M. Goula, P. Tsiakaras, J. Power Sources **126**, 16–22 (2004)
19. S.Q. Song, W.J. Zhou, Z.H. Zhou, L.H. Jiang, G.Q. Sun, Q. Xin, V. Leontidis, S. Kontou, P. Tsiakaras, Int. J. Hydrog. Energy. **30**, 995–1001 (2005)
20. C. Coutanceau, S. Brimaud, C. Lamy, J.M. Léger, L. Dubau, S. Rousseau, F. Vigier, Electrochim. Acta **53**, 6865–6880 (2008)
21. L. Jiang, A. Hsu, D. Chu, R. Chen, Int. J. Hydrog. Energy. **35**, 365–372 (2010)
22. F. Munoz, C. Hua, T. Kwong, L. Tran, T.Q. Nguyen, J.L. Haan, Appl. Catal. B. **174**, 323–328 (2015)
23. M. Simões, S. Baranton, C. Coutanceau, Appl. Catal. B. **110**, 40–49 (2011)
24. J. Nandenha, R.F.B. De Souza, M.H.M.T. Assumpcao, E.V. Spinace, A.O. Neto, Ionics **19**, 1207–1213 (2013)
25. A.O. Neto, J. Nandenha, R.F.B. De Souza, G.S. Buzzo, J.C.M. Silva, E.V. Spinacé, M.H.M.T. Assumpção, J. Fuel Chem. Technol. **42**, 851–857 (2014)
26. E.H. Fontes, R.M. Piasentin, J.M.S. Ayoub, J.C.M. da Silva, M.H.M.T. Assumpção, E.V. Spinacé, A.O. Neto, R.F.B. De Souza, Mater Renew Sustain Energy. **4**, 1–10 (2015)
27. A.O. Neto, J. Nandenha, M.H.M.T. Assumpção, M. Linardi, E.V. Spinacé, R.F.B. de Souza, Int. J. Hydrog. Energy. **38**, 10585–10591 (2013)
28. M.H.M.T. Assumpção, J. Nandenha, G.S. Buzzo, J.C.M. Silva, E.V. Spinacé, A.O. Neto, R.F.B. de Souza, J. Power Sources **253**, 392–396 (2014)
29. R.F.B. De Souza, G.S. Buzzo, J.C.M. Silva, E.V. Spinace, A.O. Neto, M.H.M.T. Assumpcao, Electrocatalysis. **5**, 213–219 (2014)
30. R.M. Modibedi, T. Masombuka, M.K. Mathe, Int. J. Hydrog. Energy. **36**, 4664–4672 (2011)
31. H. Wang, Z. Liu, S. Ji, K. Wang, T. Zhou, R. Wang, Electrochim. Acta **108**, 833–840 (2013)
32. K.J.J. Mayrhofer, J.C. Meier, S.J. Ashton, G.K.H. Wiberg, F. Kraus, M. Hanzlik, M. Arenz, Electrochem. Commun. **10**, 1144–1147 (2008)
33. R.F.B. De Souza, A.E.A. Flausino, D.C. Rascio, R.T.S. Oliveira, E.T. Neto, M.L. Calegaro, M.C. Santos, Appl. Catal. B. **91**, 516–523 (2009)
34. G.S. Pawley, J. Appl. Crystallogr. **14**, 357–361 (1981)
35. M. Wojdyr, J. Appl. Crystallogr. **43**, 1126–1128 (2010)
36. R.F.B. De Souza, L.S. Parreira, J.C.M. Silva, F.C. Simões, M.L. Calegaro, M.J. Giz, G.A. Camara, A.O. Neto, M.C. Santos, Int. J. Hydrog. Energy. **36**, 11519–11527 (2011)
37. W. Zhou, M. Li, L. Zhang, S.H. Chan, Electrochim. Acta **123**, 233–239 (2014)
38. D.Z. Jeffery, G.A. Camara, Electrochem. Commun. **12**, 1129–1132 (2010)
39. J. Schnaidt, M. Heinen, D. Denot, Z. Jusys, R. Jürgen Behm, J. Electroanal. Chem. **661**, 250–264 (2011)
40. M. Simões, S. Baranton, C. Coutanceau, Appl. Catal. B. **93**, 354–362 (2010)
41. J. Cai, H. Ma, J. Zhang, Z. Du, Y. Huang, J. Gao, J. Xu, Chin. J. Catal. **35**, 1653–1660 (2014)
42. C.A. Martins, M.J. Giz, G.A. Camara, Electrochim. Acta **56**, 4549–4553 (2011)
43. J.C.M. Silva, L.S. Parreira, R.F.B. De Souza, M.L. Calegaro, E.V. Spinacé, A.O. Neto, M.C. Santos, Appl. Catal. B. **110**, 141–147 (2011)
44. K. Miyazaki, T. Matsumiya, T. Abe, H. Kurata, T. Fukutsuka, K. Kojima, Z. Ogumi, Electrochim. Acta **56**, 7610–7614 (2011)